UNIVERSITYOF BIRMINGHAM

Ultrafast Spectroelectrochemistry of the Catechol/o-Quinone Redox Couple in Aqueous Buffer Solution

Goia, Sofia; Richings, Gareth W.; Turner, Matthew A. P.; Woolley, Jack M.; Tully, Joshua J.; Cobb, Samuel J.; Burriss, Adam; Robinson, Ben R.; Macpherson, Julie V.; Stavros, Vasilios G.

Document Version
Publisher's PDF, also known as Version of record

[Link to publication on Research at Birmingham portal](#)

Ultrafast Spectroelectrochemistry of the Catechol/o-Quinone Redox Couple in Aqueous Buffer Solution

Sofia Goia,[a, b] Gareth W. Richings,[a] Matthew A. P. Turner,[a, b, c] Jack M. Woolley,[a, d] Joshua J. Tully,[a] Samuel J. Cobb,[a, e] Adam Burriss,[f] Ben R. Robinson,[f] Julie V. Macpherson,[a] and Vasilios G. Stavros*[a, g]

Eumelanin is a natural pigment found in many organisms that provides photoprotection from harmful UV radiation. As a redox-active biopolymer, the structure of eumelanin is thought to contain different redox states of quinone, including catechol subunits. To further explore the excited state properties of eumelanin, we have investigated the catechol/o-quinone redox couple by spectroelectrochemical means, in a pH 7.4 aqueous buffered solution, and using a boron doped diamond mesh electrode. At pH 7.4, the two proton, two electron oxidation of catechol is promoted, which facilitates continuous formation of the unstable o-quinone product in solution. Ultrafast transient absorption (femtosecond to nanosecond) measurements of o-quinone species involve initial formation of an excited singlet state followed by triplet state formation within 24 ps. In contrast, catechol in aqueous buffer leads to formation of the semiquinone radical $\Delta t > 500$ ps. Our results demonstrate the rich photochemistry of the catechol/o-quinone redox couple and provides further insight into the excited state processes of these key building blocks of eumelanin.

Introduction

Eumelanin is a member of the melanin class of pigments with photoprotective properties that shield cells from harmful, phototoxic reactions, such as DNA damage initiated by UV radiation absorption of nucleobases.[1,2] This is a particularly important property as it acts as a natural human sunscreen. It is a heterogenous macromolecule with a complex structure due to the wide variety of precursor molecules that contribute to its properties, including photoexcited state decay processes.[3,4] In

[a] S. Goia, G. W. Richings, M. A. P. Turner, J. M. Woolley, J. J. Tully, S. J. Cobb, J. V. Macpherson, V. G. Stavros
Department of Chemistry, University of Warwick, Coventry, CV4 7AL, UK
E-mail: v.stavros@bham.ac.uk

[b] S. Goia, M. A. P. Turner
Molecular Analytical Science CDT, Senate House, University of Warwick, Coventry, CV4 7AL, UK

[c] M. A. P. Turner
Department of Physics, University of Warwick, Coventry, CV4 7AL, UK

[d] J. M. Woolley
Warwick Centre for Ultrafast Spectroscopy, Department of Physics, University of Warwick, Coventry, CV4 7AL, UK

[e] S. J. Cobb
Department of Chemistry, University of Cambridge, Cambridge, CB2 1EW, UK

[f] A. Burriss, B. R. Robinson
Syngenta, Warfield, Bracknell, RG42 6EY, UK

[g] V. G. Stavros
School of Chemistry, University of Birmingham, Edgbaston, Birmingham, B15 2TT, UK

this type of system, of high importance are intramolecular processes as well as intermolecular interactions between monomers. Molecules present in different redox states also take part in the excited state decay pathways of eumelanin. These could potentially affect the relaxation mechanisms of eumelanin and subsequently its photoprotective properties.[5,6] In order to study these mechanisms, transient absorption spectroscopy (TAS) was used to study the lifetimes related to the decay mechanisms observed.[5,7,8]

Eumelanin is a redox-active biopolymer,[9] with intermolecular interactions between the subunits contained within the structure of eumelanin existing in different oxidation states.[3,10,11] Notably, in the present study, our focus is on the subunits catechol and o-quinone. Catechols are widespread in biology, contributing towards numerous biological processes and constitute one of the key building blocks of eumelanin.[5,12] In our previous work, a bottom-up approach was used when studying eumelanin photoprotection, by investigating the TAS of a substituted catechol molecule.[7] Multiple decay pathways were observed upon photoexcitation of 4-tert-butylcatechol depending on the solvent used.[7] As a means to further deciphering the complex spectroscopy of catechol building blocks in a redox active environment, we break down the problem into its constituent parts by considering as a model system the catechol/o-quinone redox couple, which can undergo a proton-coupled electron transfer reaction.[13,14] The number of protons transferred depends on the protonation state of the molecule, which is controlled by pH.[14,15] For catechol, at a pH below 9, this molecule should follow a two proton, two electron oxidation to form o-quinone,[13] Figure 1.

In this paper, we expand on the previous work[5–8] performed in different solvents on the catechol and catechol/quinone heterodimer functional groups of eumelanin which investigated the intra- and intermolecular processes between

Figure 1. Redox process of catechol/o-quinone through the loss/acceptance of two protons ($2H^+$) and two electrons ($2e^-$).

monomers and interaction with the solvent. Here, we focus on both steady-state and ultrafast transient absorption spectroelectrochemical interrogation of the catechol/o-quinone redox couple, at pH 7.4 (in aqueous buffer), using a boron doped diamond (BDD)[16] mesh electrode to generate the o-quinone in-situ electrochemically. The *tert*-butyl substituted catechol and o-quinone have previously been used in experimental settings due to their higher chemical stability in solution and solubility in less polar solvents.[7,17] Here, the continuous generation of the unstable o-quinone species in aqueous solution[18] using electrochemistry provides an elegant way of changing the oxidation state of the catechol species and analysing the photophysical and photochemical properties of the redox couple.

Results and Discussion

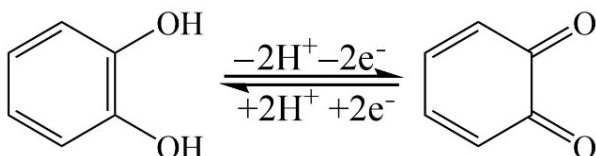### Spectroelectrochemical Set-Up and Steady-State Absorption Measurements

In the present work, the 3D printed spectroelectrochemical (SEC) cell, as presented in Figure 2a, takes advantage of a bigger headspace than the one described in our previous work.[19] This enables the use of a cover over the wire and electrical contact for the BDD electrode, through which it can be fixed onto the cell (see ESI 1, Figure S1). In this way, the electrochemical components are mechanically stabilised and continuous translation of the sample stage is also possible, which can be vital in TAS experiments due to potential photoproduct formation, depending on the system being analysed. As shown in the UV-Vis spectra in Figure 2b, in pH 7.4 aqueous buffer, catechol has an absorption maximum at 275 nm. To determine the potential needed to form the o-quinone species, cyclic voltammetry measurements were performed using the three-electrode system (see ESI 1, Figure S2) within the custom-built SEC cell, on a 5 mM catechol solution in 0.1 M phosphate buffered saline (PBS) pH 7.4 buffer, 0.2 M KCl. A potential of *ca.* 1.2 V *vs* SCE was then chosen as the oxidation peak. For steady-state measurements, after 15 mins of applied potential, a spectrum was recorded, as seen in Figure 2b, and the characteristic absorption peak of o-quinone was observed, with a maximum at 385 nm.[6,20]

The electrochemical oxidation/reduction pathways can be monitored by varying solution pH. Given the pK_a ($pK_a = 9.45$[13]) of catechol, the oxidation of catechol to o-quinone should follow a $2H^+ + 2e^-$ mechanism at pH < 9.45,[13] which can be described using the 'scheme of squares' proposed by Jacq (see
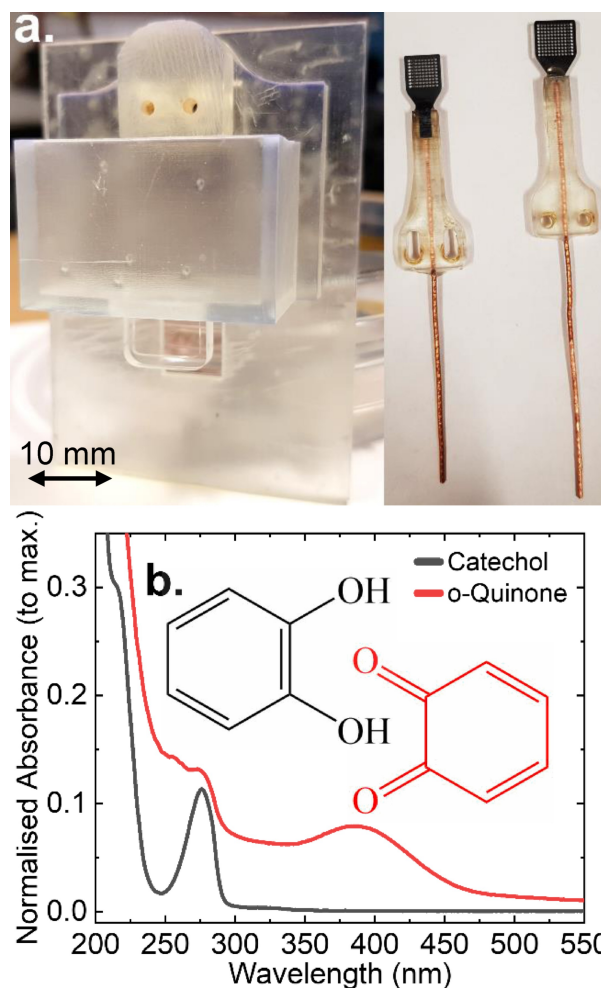
Figure 2. (a.) Photograph of the 3D printed cell and BDD mesh electrode; **(b.)** UV/Vis spectra of catechol taken using a 1 mM solution in 0.1 M PBS buffer pH 7.4, 0.2 M KCl (grey) and the electrochemically oxidised o-quinone (red, *ca.* 1.2 V *vs* SCE oxidation potential was applied for 15 minutes before recording the spectrum).

ESI 2, Figure S4).[21] From the UV/Vis spectra of the electrochemically generated o-quinone, it appears that a small concentration of catechol is still present. However, at the concentrations used within this work ($<$ 10 mM starting catechol species), we do not expect to see interaction from a potential heterodimer formation.[5]

Computational Calculations for Catechol

Initial time-dependent density functional theory (TDDFT) calculations using MOLPRO (6-311++G** basis set, PBE0 functional) were performed to identify the energy levels involved in the steady-state and ultrafast photoexcitation studies. The transitions observed for catechol are presented in ESI 3, Table S1 and Figure S5, with the peak around 275 nm (Figure 2b) being assigned to the $S_2 \leftarrow S_0$ ($\pi\pi^*$) lowest lying energy transition (see below for further details), the energy being within 10 nm of the

ChemPhotoChem

Research Article
doi.org/10.1002/cptc.202300325

Chemistry Europe
European Chemical
Societies Publishing

experimental data. Three triplet states ($\pi\pi^*$) with energies below the S_1 were also determined.

Additionally, vertical excitation energies were calculated for catechol (see ESI 3, Table S2 for the cartesian coordinates of the optimised ground state geometry) using state-averaged complete active space self-consistent field (SA-CASSCF), SA(7S,7T)-CASSCF(10,8)/6-311++G** , the results of which are presented in ESI 3, Table S3 (energies and oscillator strengths of excitation from S_0). Using this method, we see that it is the S_1 singlet state, with an excitation wavelength of 257 nm, that is closest to that of the peak in Figure 2b (at 275 nm). The five other calculated singlet excited states had excitation wavelengths between 136 and 165 nm, suggesting that they merge into the high intensity peak seen below 225 nm in the experiment. In ESI 3, Table S4, we present the characters of the excited states in terms of the orbital excitations constituting the configurations with largest coefficient in the CASSCF expansion for each state (see also ESI 3, Table S5 for pictures and energies of the active space orbitals), from which we see that the S_1 ($\pi\pi^*$) state is represented by a single HOMO to LUMO excitation. The other excited states are all of $\pi\pi^*$ character (as guaranteed by the active space, but as noted in the experimental section, the inclusion of other orbitals did not affect this), being best represented by excitations within the HOMO-1, HOMO, LUMO, and LUMO$+1$ (configurations involving other orbitals were also included, but with smaller coefficients) space.

The excitation energies of the states were refined by applying the n-electron valence state perturbation theory (NEVPT2)[22–24] method to recover the effects of dynamic electron correlation: these results are presented in ESI 3, Table S6 (again both excitation energies and oscillator strengths from S_0, although the latter are only approximate as they were derived using the CASSCF transition dipole moments, which were the only ones available). We see that the experimental peak at 275 nm is best represented by S_1 (245 nm), with the five higher energy excited states contributing to the high intensity peak around 200 nm. Two triplet states were present at a lower energy, below the S_1 state, with T_3 being within 10 nm of S_1 for both CASSCF and NEVPT2 pictures. Thus, from the results, as T_3 is in close energy proximity to S_1, the possibility of intersystem crossing is suggested, from S_1 to the triplet manifold subsequent to excitation to the S_1 state. Such a possibility is also present when exciting to higher energy singlet states, there being triplet states present of similar energy. For this work, we did not perform further calculations to improve the current results as the overall thrust of these calculations were to broadly assess which electronic states were accessed. Further calculations would benefit the analysis but go beyond the scope of the present study.

TAS of Catechol in Aqueous Buffer Solution

The decay mechanisms of catechol in an aqueous buffer solution (pH 7.4) following excitation at 275 nm were studied through TAS. The collated TA spectra in Figure 3a show positive features across the entire spectral window of our measurements
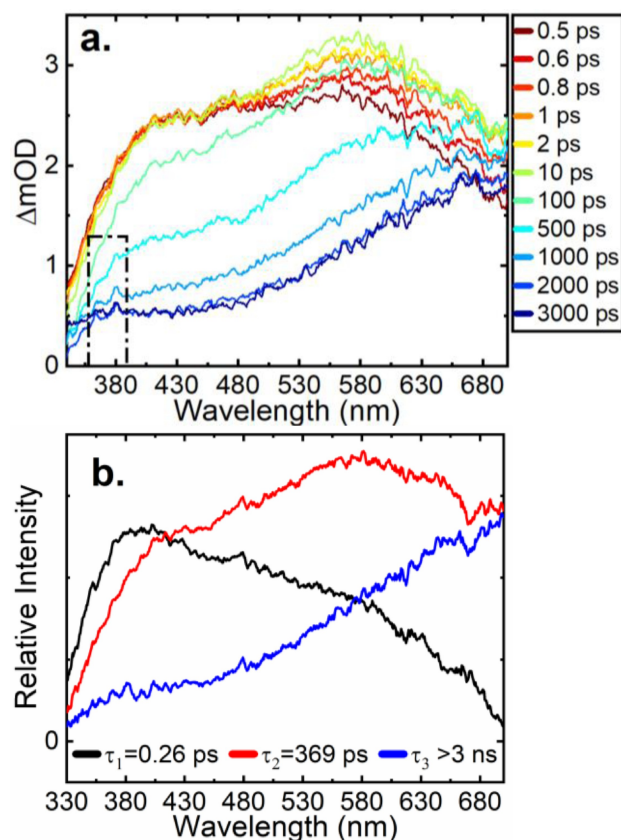

Figure 3. (**a.**) Different time delays (Δt) chosen for the TA spectra of catechol taken using a 5 mM solution in 0.1 M PBS buffer pH 7.4, 0.2 M KCl with photoexcitation at 275 nm; the semiquinone radical is highlighted by the dashed rectangle; (**b.**) The corresponding evolution-associated difference spectra (EADS) from the global fit.

(330 – 700 nm), with two main broad excited state absorption (ESA) features centred at 415 nm and 580 nm (at $\Delta t < 10$ ps). As both decay, a long-lived feature is formed at $\Delta t > 500$ ps, with peaks centred around 380 nm (with a smaller peak around 365 nm) and 670 nm, which persists beyond the maximum time-window of our experiments ($\Delta t = 3$ ns). To note, the data used in Figure 3a was specifically acquired to highlight the features observed, as described in the experimental section. The global sequential fit using the Glotaran package[25] employed to extract the lifetimes of the processes contained in the TA spectra returns three time-constants: $\tau_1 = 0.26 \pm 0.09$ ps, $\tau_2 = 368.8 \pm 6.3$ ps, and $\tau_3 > 3$ ns, plotted as evolution-associated difference spectra (EADS)[26] shown in Figure 3b, with the associated residuals plot (ESI 4, Figure S7a) demonstrating the agreement between the fitted and the experimental data. Moreover, single wavelength transient slices were plotted at 380 nm and 580 nm, with the extracted global sequential fit traces superimposed to show the quality of the fit (ESI 4, Figure S8a and b). Solvent-only scans retrieved an instrument response of ≈ 180 fs (ESI 4, Figure S9a) and single photon-initiated dynamics were confirmed (ESI 4, Figure S10a). The excited state dynamics of catechol (pH 7.4) following photoexcitation at 275 nm are assigned as follows: τ_1 is attributed to intramolecular vibrational energy transfer along with solvent

ChemPhotoChem

Research Article
doi.org/10.1002/cptc.202300325

**Chemistry
Europe**
European Chemical
Societies Publishing

rearrangement; τ_2 is attributed to (mainly) internal conversion as well as O—H dissociation (semiquinone radical formation) and intersystem crossing; and τ_3 is attributed to the lifetime of the solvated electron along with the semiquinone radical and a possible triplet state (ESI 4, Figure S11). At 5 mM it is assumed that the solution predominantly contains the monomer form of catechol.[5,8] Previous work on the catechol monomer in acetonitrile[7] (polar solvent) observed a similar timescale for τ_1, attributed to intramolecular vibrational energy transfer along with solvent rearrangement, pathways likely to take place within the current studies as well.

The second time constant τ_2, is a factor of two less than that previously observed in catechol/acetonitrile.[8] In line with this work, we assign τ_2 to depletion of the S_1 excited state. The large difference in this finding with this previous study is unsurprising; the ultrafast dynamics of catechol are known to be greatly influenced by the solvent environment,[5,7,8] with various competing decay mechanisms being possible, as upon excitation of the S_1 state, O—H dissociation or internal conversion to the ground state (S_0) can take place. At this junction, it is also worth noting that, in aqueous buffer solution, we observe formation of the semiquinone radical (see ESI 2, Figure S4), which can be identified by a very small, albeit noticeably sharp absorption feature at 380 nm (and the smaller peak around 365 nm)[27–30] at longer time delays, slowly starting to appear from $\Delta t > 500$ ps.

We now discuss the origin of the third lifetime, with time constant τ_3. The broad absorption feature appearing > 500 nm points towards the presence of a solvated electron.[31–36] In order to confirm (or dismiss) this, further experiments were performed in the presence of an electron scavenger, KNO_3 (0.25 M); KNO_3 is able to diffusively scavenge solvated electrons.[32,37] Figure 4 compares a 2 ns TA spectrum with (red) and without (black) the presence of KNO_3. It is clear that the addition of KNO_3 removes the broad absorption feature appearing > 500 nm. Thus, we assign τ_3 as the lifetime of the solvated electron, which persists beyond the maximum time-window of our experiments ($\Delta t = 3$ ns).
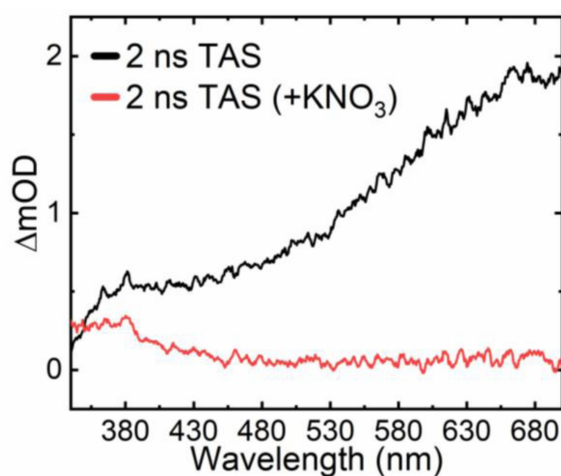

Figure 4. 2 ns TAS taken using a 5 mM solution of catechol in 0.1 M PBS buffer pH 7.4, 0.2 M KCl and with addition of 0.25 M KNO₃ (photoexcitation at 275 nm).

Interestingly, the addition of KNO_3 accentuates the semiquinone radical formation as well as the broad absorption that the radical feature straddles, with a tail that extends up to ~480 nm. Depletion of the singlet excited state (τ_2 ~370 ps) via intersystem crossing to a triplet state is possible, though masked by the formation of the solvated electron. From our calculations, at least two potential triplet states could be accessed with energies below S_1. The broad absorption feature seen in Figure 4 could thus also be attributed to the presence of a triplet state which would be in keeping with previous studies which have identified triplet state absorption between 340 to 480 nm.[35]

Computational Calculations for o-Quinone

Initial TDDFT calculations using MOLPRO (6-311++G** basis set, PBE0 functional) were also performed for o-quinone. The transitions observed, presented in ESI 3 Table S1 and Figure S6, show the first bright state at a lower energy peak around 444 nm, blue-shifted compared to the experimental data (Figure 2b) by *ca.* 60 nm, which was assigned to a $S_3 \leftarrow S_0$ ($\pi\pi^*$) transition. The second bright state at a higher energy level, was observed at 261 nm and it was also assigned to a $\pi\pi^*$ transition. Compared to the results obtained for catechol, the TDDFT calculations for o-quinone do not match the experimental data very well.

To further aid interpretation of the behaviour of o-quinone, SA(15S,15T)-CASSCF(12,10)/6-311++G** calculations were performed to obtain the vertical excitation energies, from S_0 (see ESI 3, Table S2 for the cartesian coordinates of the optimised geometry), at the Franck-Condon point; the results are presented in ESI 3, Table S3 along with the oscillator strengths of the transitions. From these results, we see that the lowest energy bright state is S_4 at an excitation wavelength of 225 nm; a result in poor agreement with experiment (Figure 2b). Looking at Table S7 and S8 in ESI 3, we see that S_4 is characterised by a configuration containing a double excitation from HOMO -1 to the LUMO, *i.e.* the state is $\pi\pi^*$, whereas the lower energy states (closer to the experimental peak) are all dark states of $n\pi^*$ character.

To further investigate this poor agreement, the NEVPT2 method was applied to each state, in order to account for the dynamic electron correlation missing from the SA-CASSCF calculation. The results of these calculations are given in ESI 3, Table S6, where we now find a bright, $\pi\pi^*$ state (S_3) with a vertical excitation wavelength of 363 nm, which agrees fairly well with the peak just below 400 nm in the experiment. From Table S5 we see that the NEVPT2 S_3 state resulted from a correction to the CASSCF S_6 state; the dynamic correlation in this state must be large in relation to that in the lower energy states, hence its significant decrease in relative energy, bringing it in line with the experimental result. As with catechol, for the NEVPT2 results there are three triplet states lower in energy than the first, bright singlet state. T_3 is at a wavelength only 28 nm higher than S_3, so there is potential for deactivation by intersystem crossing after excitation to S_3. However, unlike the

ChemPhotoChem

Research Article
doi.org/10.1002/cptc.202300325

**Chemistry
Europe**

European Chemical
Societies Publishing

case with catechol, there are also two lower energy singlet states. These may provide an internal conversion pathway by which energy could be dissipated; indeed, the overall path could be a mix of both processes.

TAS of o-Quinone in Aqueous Buffer Solution

We now focus on the ultrafast dynamics of the electrochemically generated o-quinone. From the TA spectra presented in Figure 5a (TAS data was again pixel averaged, as described in the experimental section), an initial broad ESA ($\Delta t < 1$ ps) covers the entire available spectral range of the white light probe, exhibiting a smaller peak around 460 nm and a broader one around 580 nm. As the ESA decays, a narrower feature of small intensity forms, with a peak centred around 540 nm, which persists to $\Delta t = 3$ ns. A negative feature around 450 nm is also present; the intensity of this feature drops slightly in the first 10–20 ps, and it remains constant thereafter. The negative feature around 400 nm is likely due to ground state bleach (GSB). The dip in intensity around 450 nm could thus be caused by a trapped population in a singlet excited state (S_n) or a triplet state (T_n), with an ESA above the GSB in the same region at early time, which would in turn result in a negative feature within the TA spectra.[39] The TA spectra were again fitted using
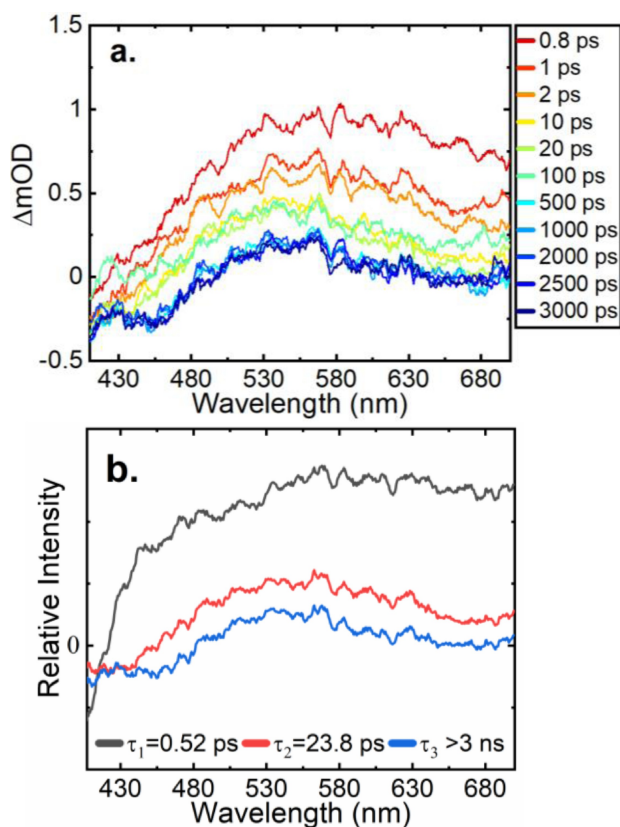

Figure 5. (a.) Different time delays (Δt) chosen for the TA spectra of electrochemically generated o-quinone (*ca.* 1.2 V *vs* SCE) taken using a 5 mM solution of catechol in 0.1 M PBS buffer pH 7.4, 0.2 M KCl with photoexcitation at 385 nm; **(b.)** The corresponding evolution-associated difference spectra (EADS) from the global fit.

a global sequential model yielding four time constants, though the first time constant (*ca.* 40 fs) was needed in order to cover artefacts from the quartz cuvette. The following time constants were recovered for the electrochemically generated o-quinone: $\tau_1 = 0.52 \pm 0.07$ ps, $\tau_2 = 23.8 \pm 2.3$ ps, and $\tau_3 > 3$ ns, plotted as EADS in Figure 5b, with the associated residuals plot found in ESI 4, Figure S7b. Single wavelength transient slices at 550 nm and 670 nm and the extracted global sequential fit traces were also plotted (ESI 4, Figure S8c and d). To note, the low signal-to-noise ratio observed within our experiments means the uncertainty within the time constants acquired is likely an underestimate. Solvent-only scans retrieved an instrument response of ≈ 130 fs (ESI 4, Figure S9b) and single photon-initiated dynamics were confirmed (ESI 4, Figure S10b). In terms of the excited state dynamics of o-quinone (pH 7.4) following photoexcitation at 385 nm, we assign the time constants as follows: τ_1 is attributed to the lifetime of an excited singlet state; τ_2 is attributed to a possible population of a new excited state (likely a triplet state); and τ_3 is attributed to the lifetime of the newly populated state (ESI 4, Figure S11).

To assign the time constants to specific decay pathways, we draw reference to a previous TAS study performed by Grieco *et al.*[6] on the 3,5-di-*tert*-butyl substituted o-quinone, in cyclohexane and 2-propanol. Briefly, in this study, population of the S_n excited state was observed (0.5 ps), followed by rapid intersystem crossing to a triplet state T_n (3.8 and 7.7 ps), which persisted beyond the observation window; a similar decay pathway seems to be taken in the 2-propanol solution.[6] By comparing the spectra of the o-quinone monomer in the present study, with the spectra acquired from the o-quinone + catechol heterodimer (by Grieco *et al.*[6]), and considering the initial concentration of catechol used, it appears that the features acquired within our TAS shown in Figure 5, are mainly from the o-quinone monomer. In the present study, the first time constant $\tau_1 = 0.52 \pm 0.07$ ps could be assigned to the lifetime of an excited singlet state (S_n) of o-quinone. The striking difference between τ_1 and τ_2 points towards (but is not definitive) a new excited state being populated. Considering the results published previously, it is likely that population of a triplet state[40] is described by $\tau_2 = 23.8 \pm 2.3$ ps, though it is unknown whether intersystem crossing is preceded by an internal conversion to the lowest lying S_n. The presence of lower lying nπ* states within o-quinone suggests that internal conversion could precede the intersystem crossing to the triplet state. Thus, the third time constant, τ_3, is assigned as the lifetime of the formed triplet state, which persists beyond $\Delta t = 3$ ns.

The decay pathways of catechol and o-quinone in aqueous buffer (pH 7.4) appear to comprise a multitude of competing mechanisms. For catechol, the formation of the solvated electron seemed to have an effect on the lifetime of the singlet excited state, with possible triplet state formation somewhat masked by the long-lived solvated electron as seen in the measurements with KNO₃. In contrast, the o-quinone monomer photodynamics shows the formation of a long-lived triplet state, very similar to the decay pathways observed previously by Grieco *et al.*[6] Within the present work, however, the

ChemPhotoChem

Research Article
doi.org/10.1002/cptc.202300325

Chemistry Europe
European Chemical
Societies Publishing

investigation into the excited state relaxation processes of o-quinone itself was possible through electrochemical generation of the species of interest.

Conclusions

Transient absorption spectroscopy of the catechol/o-quinone redox couple in aqueous buffer solution (pH 7.4) was studied using a spectroelectrochemical methodology incorporating a boron doped diamond mesh electrode. The transient absorption spectroelectrochemistry method offers an accessible approach to electrochemically generate and analyse unstable redox species, here o-quinone, without the need of using substituted compounds. The present study performed in an aqueous solvent adds to the increasing knowledge of the excited-state decay pathways of the catechol/o-quinone monomer building blocks present in eumelanin. The formation of long-lived solvated electrons was demonstrated within the decay pathways of photoexcited catechol using KNO_3 as a scavenger. In addition to the solvated electron formation, it appears that multiple decay pathways are present, including the detection of the semiquinone radical at 380 nm ($\Delta t >$ 500 ps) and triplet state formation. The decay mechanisms of the o-quinone species included population of an excited state (S_n) within *ca.* 0.5 ps and formation of a long-lived triplet state that persisted to the maximum $\Delta t > 3$ ns of our instrument. The possibility of deactivation of the excited state *via* a triplet state was observed for both the catechol and o-quinone molecules, the triplet manifold being energetically accessible from the optically bright states.

Our present study demonstrates that triplet states and radicals are formed upon light irradiation; these can in turn potentially become reactive species within eumelanin pigments and, subsequently, could lead to role reversal of eumelanin, from being photoprotective to being phototoxic.[29,35] For instance, such phototoxicity could arise from eumelanin acting as a photosensitiser following absorption of UV radiation; this could lead to the generation of reactive oxygen species resulting in DNA strand breakage.[1] Future work within our group will focus on investigating semiquinone radicals further. As chromophores with different oxidation states have a key role in the ultrafast decay pathways upon photoexcitation of eumelanin, this could shed more light on the role of eumelanin in humans and help further the research into more efficient sunscreens.[12] For example, the semiquinone radical is thermodynamically inaccessible in aqueous solution under electrochemical control. By modifying the spectroelectrochemical set-up such that aprotic solvents could be used in the cell, we plan to drive the reaction towards semiquinone formation,[41] enabling us to study the photoexcited decay pathways of the semiquinone radical. This could, in turn, shed more light on possible further reactions of the semiquinone radical. In so doing, additional insight into the photochemistry and photophysics of eumelanin could be explored, and thus its properties within organisms.

Experimental Section

Materials and Equipment

Solutions were prepared using the following chemicals: catechol ($\geq$ 99%, Acros Organics), potassium chloride (analytical reagent grade, VWR Chemicals), PBS tablets (Sigma-Aldrich, pH 7.4, 1 tablet/200 mL), potassium nitrate (ACS reagent $\geq$ 99.0%, Sigma-Aldrich). All chemicals were used as received without any further purification. Deionised (DI) water with a resistivity of 18.2 MΩcm was used throughout all experiments. For each measurement, the solutions were freshly prepared, and experiments were performed at room temperature (20 °C $\pm$ 2 °C).

Steady-state absorption measurements were conducted using a Cary 60 UV/Vis Spectrophotometer (Agilent Technologies, US). Time-resolved measurements were conducted using the transient absorption spectroscopy instrumentation available at the Warwick Centre for Ultrafast Spectroscopy (https://warwick.ac.uk/research/rtp/wcus/). Electrochemical measurements were performed using a PalmSens EmStat3 potentiostat.

BDD Working Mesh Electrode and SEC Cell

The process through which the spectroelectrochemical cell and the working electrode were fabricated has been previously reported in detail.[19] Through this work the following upgrades were performed to our previous study:[19] the design of the cell and electrode was modified to have a 3D printed covering over the Cu wire and electrode contact. The Cu wire was connected to the BDD electrode using a conductive epoxy (Silver Epoxy, Circuitworks, USA). The SEC cell and the housing for the BDD electrode were 3D printed using a clear resin (Clear, FormLabs) material. This housing allowed the electrode to be fixed to the cell using screws, to prevent unwanted movement, and it was also used to isolate the Cu wire from the electrolyte solution. A 1 mm pathlength quartz cuvette, through which the UV/visible light was passed, was also attached to the bottom of the 3D printed cell headspace using an epoxy resin. The thickness of the BDD electrode was 0.5 mm, and the holes within the electrode had a diameter of 0.5 mm and a 0.55 mm centre to centre space (see ESI 1, Figure S1 for details).

Oxidation of Catechol

A three-electrode system (SCE reference electrode, Pt wire counter electrode, BDD mesh working electrode) was used throughout all electrochemical measurements and an inert atmosphere was kept by bubbling the solution with N_2. For steady-state spectroelectrochemical experiments, cyclic voltammetry (CV) measurements were performed on a 5 mM catechol solution (0.1 M PBS buffer pH 7.4, 0.2 M KCl) at a 0.1 V s^{-1} scan rate between -1.0 V and 2.0 V *vs* SCE (see ESI 1, Figure S2 for details). From this CV an oxidation potential of *ca.* 1.2 V *vs* SCE was chosen to drive the oxidation. The potential was applied throughout the experiment; however, there was an initial period of 15 mins where no spectral data was taken in order to ensure sufficient conversion of catechol to o-quinone, as was the case in our previous work with the initial spectroelectrochemical set-up built.[19]

Transient Absorption Spectroscopy

TAS measurements were performed on pH 7.4 aqueous buffered solutions (0.1 M PBS buffer, 0.2 M KCl) containing 5–10 mM catechol, with the concentration chosen in order to optimise the TAS signal. For catechol, a 1 mm quartz cuvette was employed and

ChemPhotoChem

Research Article
doi.org/10.1002/cptc.202300325

Chemistry Europe
European Chemical
Societies Publishing

the sample stage was continuously translated vertically and horizontally; the solution was replaced and the cuvette was cleaned after three scans in order to avoid surface aggregation on the window of the cuvette.[8] For o-quinone, the built SEC 1 mm path length static cell was used, with the sample stage being translated from 'hole-to-hole' throughout the scans. The cell had to be dismantled, as for catechol, and the components had to be cleaned after 3–4 scans (approximately 45 minutes) due to electrode fouling[42] and build-up of a thin, brown film on the surface of the BDD electrode and on the window of the cuvette in the region of the BDD electrode's position (see ESI 1, Figure S3). The accumulation of the thin film was likely due to photoproducts (polymeric in nature) derived from o-quinone.[17] Thus, to minimise irradiation of one area which would inevitably lead to increased photoproduct formation, the hole-to-hole translation of the sample stage on the×and y axes was of utmost importance for the redox couple studied. Electrode fouling was also tracked by closely monitoring the chronoamperometry trace for any changes. The TAS spectrum at 'time zero' and 1 ps delay was also monitored after each scan for any observed signal changes, to ensure consistency across measurements.

The TAS[39] set-up used has been described in detail previously.[43] For catechol, a 275 nm excitation beam at 500 µW was used, and for o-quinone, a 385 nm excitation beam at 800 µW. Solvent-only scans of the pH 7.4 buffer (0.2 M KCl) solution to determine potential contributions from the solvent and quartz cuvette were also taken using the same parameters. Due in part to the spectroelectrochemical set-up and the low intensity of the acquired signal, a low signal-to-noise ratio was apparent throughout the TAS experiments. To highlight the features observed and for plotting purposes, measurements consisting of only certain time delays were taken for catechol over 20 scans to improve the signal-to noise ratio and thus bring out the changes in spectral features more clearly. In addition, the 'smoothing' option (pixel averaging) within the KOALA software[44] was also used in this respect for plotting of the catechol and o-quinone TAS data, Figure 3a and Figure 5a, respectively. Furthermore, for plotting purposes, the corresponding global fitting extracted from the raw (unsmoothed) data, presented in Figure 3b and Figure 5b, was also pixel averaged using the 'smoothing' option in the KOALA software. The retrieved TA spectra were analysed using the Glotaran software[25] for the R package TIMP.[45] The lifetimes contained in the spectra were extracted using a global sequential fit ($A \xrightarrow{\tau_1} B \xrightarrow{\tau_2} C \xrightarrow{\tau_n} \ldots$). Single wavelength transient slices along with the corresponding extracted fit traces from the global sequential model are also plotted for both catechol (380 nm and 580 nm) and o-quinone (550 nm and 670 nm) at key features observed within the TA spectra, in order to show the quality of the fit (See ESI 4, Figure S8). The instrument response retrieved yielded full width half maximum[46] values of $\approx$180 fs (pump at 275 nm) and $\approx$130 fs (pump at 385 nm), see ESI 4, Figure S9. Pump power dependence measurements (0.15 mW – 1.5 mW and 0.2 mW – 1.8 mW for catechol and o-quinone, respectively) were performed by varying the output power of the TOPAS, and up to five-points measurements taken at varying powers. We note that single photon-initiated dynamics were confirmed by plotting the log(power) against the log(signal) across a 10 nm spectral integration window at a given Δt, and the slope of the linear fit was calculated, ESI 4, Figure S10.

Computational Calculations

TDDFT: Initial geometry optimisations were performed in gas-phase using the Molpro package[47,48] at the 6–311++G**/PBE0[49–51] level of theory. The first 10 excited states (S_n) were then calculated at the Franck-Condon geometry, using the same level of theory. Triplet state calculations were additionally performed for both molecules at the same level of theory.

CASSCF: In addition to the TDDFT calculations, vertical excitation energies were also found using the CASSCF method as implemented in MOLPRO.[47,48,52,53] For both catechol and o-quinone, geometry optimisations were performed, followed by frequency calculations to confirm that the optimised geometries indeed represented energy minima. These initial calculations used the single state CASSCF method, whilst the subsequent evaluations of the vertical excitations at the Franck-Condon points were carried out using state-averaged (SA) CASSCF. The active spaces chosen for the two molecules included all π and π^* molecular orbitals, and for o-quinone the two non-bonding lone pair orbitals on the oxygen atoms were also included, resulting in 10 electrons in 8 orbitals (CASSCF(10,8)) for catechol and 12 electrons in 10 orbitals for o-quinone (CASSCF(12,10)). For the excitation energies, 7 singlet states and 7 triplets were included in the state-averaging for both molecules giving, for catechol, SA(7S,7T)-CASSCF(10,8) and, for o-quinone, SA(7S,7T)-CASSCF(12,10). We note, after running test calculations with a larger active space, that it was found to be unnecessary to include the lone pair orbitals in the active space for catechol as they gave, at most, very small contributions to the excited states (depending on the number of states included, these orbitals could also be rotated out of the active space entirely). Subsequent to the SA-CASSCF calculations on both molecules, MOLPRO was used to perform NEVPT2 (second-order n-electron valence state perturbation theory) calculations for all resulting states in order to account for the dynamic correlation present in the molecules.[22–24,47,48]

Supporting Information

Further details on the spectroelectrochemical set-up used and the electrochemical measurements performed, along with additional TAS data and the results obtained from the computational calculations, are included in the Supporting Information.

ChemPhotoChem

Research Article
doi.org/10.1002/cptc.202300325

Chemistry Europe
European Chemical
Societies Publishing

Conflict of Interests

The authors declare no conflict of interest.

Data Availability Statement

The data that support the findings of this study are available from the corresponding author upon reasonable request.

[1] A. Büngeler, B. Hämisch, O. I. Strube, *Int. J. Mol. Sci.* **2017**, *18*.
[2] M. Brenner, J. V. Hearing, *Photochem. Photobiol.* **2008**, *84*, 539–549.
[3] E. Kim, L. Panzella, A. Napolitano, G. F. Payne, *J. Invest. Dermatol.* **2020**, *140*, 537–543.
[4] S. Ito, *Biochim. Biophys. Acta, Gen. Subj.* **1986**, *883*, 155–161.
[5] C. Grieco, F. R. Kohl, Y. Zhang, S. Natarajan, L. Blancafort, B. Kohler, *Photochem. Photobiol.* **2019**, *95*, 163–175.
[6] C. Grieco, J. M. Empey, F. R. Kohl, B. Kohler, *Faraday Discuss.* **2019**, *216*, 520–537.
[7] M. D. Horbury, L. A. Baker, W. D. Quan, J. D. Young, M. Staniforth, S. E. Greenough, V. G. Stavros, *J. Phys. Chem. A* **2015**, *119*, 11989–11996.
[8] M. A. P. Turner, R. J. Turner, M. D. Horbury, N. D. M. Hine, V. G. Stavros, *J. Chem. Phys.* **2019**, *151*, 084305.
[9] C. Grieco, F. R. Kohl, A. T. Hanes, B. Kohler, *Nat. Commun.* **2020**, *11*, 1–9.
[10] S. Ito, K. Wakamatsu, T. Sarna, *Photochem. Photobiol.* **2018**, *94*, 409–420.
[11] A. Corani, A. Huijser, T. Gustavsson, D. Markovitsi, P. Å Malmqvist, A. Pezzella, M. D'Ischia, V. Sundström, *J. Am. Chem. Soc.* **2014**, *136*, 11626–11635.
[12] F. Solano, *Molecules* **2020**, *25*, 1–18.
[13] Q. Lin, Q. Li, C. Batchelor-McAuley, R. G. Compton, *J. Phys. Chem. C* **2015**, *119*, 1489–1495.
[14] D. R. Weinberg, C. J. Gagliardi, J. F. Hull, C. F. Murphy, C. A. Kent, B. C. Westlake, A. Paul, D. H. Ess, † Dewey, G. Mccafferty, T. J. Meyer, *Chem. Rev.* **2012**, *112*, 4016–4093; Dewey, G. Mccafferty, T. J. Meyer, *Chem. Rev.* **2012**, *112*, 4016–4093.
[15] R. S. K. A. Gamage, A. J. McQuillan, B. M. Peake, *J. Chem. Soc. Faraday Trans.* **1991**, *87*, 3653–3660.
[16] J. V. Macpherson, *Phys. Chem. Chem. Phys.* **2015**, *17*, 2935–2949.
[17] C. Grieco, A. T. Hanes, L. Blancafort, B. Kohler, *J. Phys. Chem. A* **2019**, *123*, 5356–5366.
[18] H. R. Zare, M. Eslami, M. Namazian, *Electrochim. Acta* **2011**, *56*, 2160–2164.
[19] S. Goia, M. A. P. Turner, J. M. Woolley, M. D. Horbury, A. J. Borrill, J. J. Tully, S. J. Cobb, M. Staniforth, N. D. M. Hine, A. Burriss, J. V. Macpherson, B. R. Robinson, V. G. Stavros, *Chem. Sci.* **2022**, *13*, 486–496.
[20] N. Vân Anh, R. M. Williams, *Photochem. Photobiol. Sci.* **2012**, *11*, 957–961.
[21] J. Jacq, *J. Electroanal. Chem. Interfacial Electrochem.* **1971**, *29*, 149–180.
[22] C. Angeli, R. Cimiraglia, S. Evangelisti, T. Leininger, J. P. Malrieu, *J. Chem. Phys.* **2001**, *114*, 10252.
[23] C. Angeli, R. Cimiraglia, J. P. Malrieu, *J. Chem. Phys.* **2002**, *117*, 9138–9153.
[24] C. Angeli, M. Pastore, R. Cimiraglia, *Theor. Chem. Acc.* **2007**, *117*, 743–754.
[25] J. Snellenburg, S. Laptenok, R. Seger, K. Mullen, I. Van Stokkum, *J. Stat. Softw.* **2012**, *49*, 1–22.
[26] I. H. M. Van Stokkum, D. S. Larsen, R. Van Grondelle, *Biochim. Biophys. Acta* **2004**, *1657*, 82–104.
[27] E. J. Land, G. Porter, *Trans. Faraday Soc.* **1963**, *59*, 2016–2026.
[28] O. Brede, S. Kapoor, T. Mukherjee, R. Hermann, S. Naumov, *Phys. Chem. Chem. Phys.* **2002**, *4*, 5096–5104.
[29] M. Gauden, A. Pezzella, L. Panzella, A. Napolitano, M. D'Ischia, V. Sundstro, *J. Phys. Chem. B* **2009**, *113*, 12575–12580.
[30] E. J. Land, G. Porter, E. Strachan, *Trans. Faraday Soc.* **1961**, *57*, 1885–1893.
[31] Y. Kimura, J. C. Alfano, P. K. Walhout, P. F. Barbara, *J. Phys. Chem.* **1994**, *98*, 3450–3458.
[32] X. Chen, D. S. Larsen, S. E. Bradforth, I. H. M. Van Stokkum, *J. Phys. Chem. A* **2011**, *115*, 3807–3819.
[33] T. A. A. Oliver, Y. Zhang, A. Roy, M. N. R. Ashfold, S. E. Bradforth, *J. Phys. Chem. Lett.* **2015**, *6*, 4159–4164.
[34] G. Kumar, A. Roy, R. S. McMullen, S. Kutagulla, S. E. Bradforth, *Faraday Discuss.* **2018**, *212*, 359–381.
[35] C. Grieco, F. R. Kohl, B. Kohler, *Photochem. Photobiol.* **2023**, *99*, 680–692.
[36] J. J. Nogueira, A. Corani, A. El Nahhas, A. Pezzella, M. D'Ischia, L. González, V. Sundström, *J. Phys. Chem. Lett.* **2017**, *8*, 1004–1008.
[37] T. W. Kee, D. H. Son, P. Kambhampati, P. F. Barbara, *J. Phys. Chem. A* **2001**, *105*, 8434–8439.
[38] D. V. Bent, E. Hayon, *J. Am. Chem. Soc.* **1975**, *97*, 2599–2606.
[39] R. Berera, R. van Grondelle, J. T. M. Kennis, *Photosynth. Res.* **2009**, *101*, 105–118.
[40] S. M. Hubig, T. M. Bockman, J. K. Kochi, *J. Am. Chem. Soc.* **1997**, *119*, 2926–2935.
[41] M. T. Huynh, C. W. Anson, A. C. Cavell, S. S. Stahl, S. Hammes-Schiffer, *J. Am. Chem. Soc.* **2016**, *138*, 15903–15910.
[42] M. Lutz, E. Burestedt, J. Emnéus, H. Lidén, S. Gobhadi, L. Gorton, G. Marko-Varga, *Anal. Chim. Acta* **1995**, *305*, 8–17.
[43] J. M. Woolley, M. Staniforth, M. D. Horbury, G. W. Richings, M. Wills, V. G. Stavros, *J. Phys. Chem. Lett.* **2018**, *9*, 3043–3048.
[44] M. P. Grubb, A. J. Orr-Ewing, M. N. R. Ashfold, *Rev. Sci. Instrum.* **2014**, *85*.
[45] K. M. Mullen, I. H. M. Van Stokkum, *J. Stat. Softw.* **2007**, *18*, 1–46.
[46] S. A. Kovalenko, A. L. Dobryakov, J. Ruthmann, N. P. Ernsting, *Phys. Rev. A* **1999**, *59*, 2369–2384.
[47] H.-J. Werner, P. J. Knowles, G. Knizia, F. R. Manby, M. Schutz, *WIREs Comput. Mol. Sci.* **2012**, *2*, 242–253.
[48] H.-J. Werner, P. J. Knowles, G. Knizia, F. R. Manby, M. Schütz, P. Celani, W. Györffy, D. Kats, T. Korona, R. Lindh, A. Mitrushenkov, G. Rauhut, K. R. Shamasundar, T. B. Adler, R. D. Amos, A. Bernhardsson, A. Berning, D. L. Cooper, M. J. O. Deegan, A. J. Dobbyn, F. Eckert, E. Goll, C. Hampel, A. Hesselmann, G. Hetzer, T. Hrenar, G. Jansen, C. Köppl, Y. Liu, A. W. Lloyd, R. A. Mata, A. J. May, S. J. McNicholas, W. Meyer, M. E. Mura, A. Nicklass, D. P. O'Neill, P. Palmieri, D. Peng, K. Pflüger, R. Pitzer, M. Reiher, T. Shiozaki, H. Stoll, A. J. Stone, R. Tarroni, T. Thorsteinsson, M. Wang, "MOLPRO, version 2015.1, a package of ab initio programs," can be found under http://www.molpro.net, **2015**.
[49] J. P. Perdew, M. Ernzerhof, K. Burke, *J. Chem. Phys.* **1996**, *105*, 9982–9985.
[50] C. Adamo, V. Barone, *J. Chem. Phys.* **1999**, *110*, 6158–6170.
[51] R. Krishnan, J. S. Binkley, R. Seeger, J. A. Pople, *J. Chem. Phys.* **1980**, *72*, 650–654.
[52] H. J. Werner, P. J. Knowles, *J. Chem. Phys.* **1985**, *82*, 5053–5063.
[53] P. J. Knowles, H. J. Werner, *Chem. Phys. Lett.* **1985**, *115*, 259–267.

RESEARCH ARTICLE

The transient absorption spectroelectrochemistry of the catechol/o-quinone redox couple was studied in aqueous buffer solution. This method offers an accessible approach to electrochemically generate and analyse unstable redox species, here o-quinone. The possibility of deactivation of the excited state *via* a triplet state was observed for both the catechol and o-quinone molecules, with the semiquinone radical and solvated electron also being observed in the excited state decay pathways of catechol.
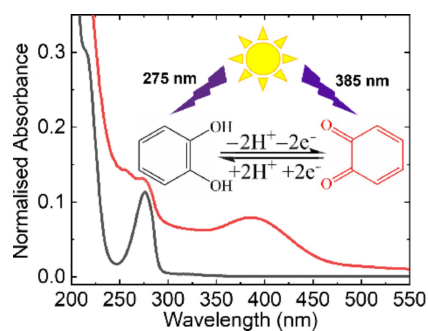
S. Goia, G. W. Richings, M. A. P. Turner, J. M. Woolley, J. J. Tully, S. J. Cobb, A. Burriss, B. R. Robinson, J. V. Macpherson, V. G. Stavros*

1 – 9

Ultrafast Spectroelectrochemistry of the Catechol/o-Quinone Redox Couple in Aqueous Buffer Solution